

Fundamental Mechanisms of Lithographic Printing Plate Imaging by Near-Infrared Lasers

David E. Hare,* Stuart T. Rhea, and Dana D. Dlott**

University of Illinois at Urbana Champaign, Box 01-6 CLSB, 600 S. Mathews Ave., Urbana, Illinois 61801

Richard J. D'Amato and Thomas E. Lewis

Presstek, Inc., 8 Commercial St., Hudson, New Hampshire 03051

The fundamental mechanisms of exposure by near-infrared pulses of multilayer films, which can be used as lithographic printing plates, are investigated using time-resolved optical microscopy. The films were developed by Presstek, Inc. (Hudson, NH) for use in the PEARL™ imaging system. Exposure by 10- μ s duration Gaussian profile pulses is shown to occur with an extremely sharp fluence threshold of $J_{th} = 0.34 \text{ J/cm}^2$. Exposure greatly alters the surface affinity for inks. Time-resolved microscopy shows the mechanism of surface alteration to involve thermochemical decomposition of the surface coating material, which results in its debonding from the film. Using threshold measurements and a theoretical thermal conduction model, debonding is shown to occur when the temperature in the film is about 500°C.

Journal of Imaging Science and Technology, 41: 291–300 (1997)

Introduction

In this paper, we describe experimental and theoretical investigations of the fundamental mechanisms of lithographic printing plate imaging by pulses from a near-infrared (near-IR) laser. In the last few years, there has been keen interest in “computer-to-plate” or “computer-to-press” systems, where a document or graphic stored in a computer is written directly to a printing plate (off-press imaging) or to a plate mounted on a printing press (on-press imaging). One way this direct imaging process can be accomplished is to use a printing plate with an ink adhesive layer (such as a silicone polymer), which can be removed by the action of intense focused laser pulses. This concept has been discussed in the literature for about twenty years.^{1–5} One such-system^{4,5} (PEARL™) has been developed, patented, and commercialized by Presstek, Inc. (Hudson, NH). The PEARL™ system can use several types of imaging materials suitable for offset lithography, which are exposed by a bank of solid-state diode lasers (In GaAlAs lasers).⁴ Other laser sources may also be used, especially a solid-state laser with higher power than a single diode laser, such as a diode-pumped Nd:YAG laser.

The fundamental mechanisms of these direct imaging materials are sufficiently complicated to warrant a systematic study. In all the silicone plate systems mentioned before, the laser pulses were not directly absorbed by the silicone coating itself, but instead by an absorbing underlayer. In the system described by Nechiporenko and Markova in 1978,¹ a carbon dioxide laser pulse is absorbed by a lacquer underlayer. It was claimed that vaporization of the lacquer layer tears apart the ink adhesive layer. In the system described by Eames in 1979,² a Nd:YAG laser pulse is absorbed in an underlayer containing carbon black and nitrocellulose, which presumably acts in a manner similar to the lacquer layer mentioned previously. In 1980, another related system was described³ where Nd:YAG pulses are absorbed in a thin film metallic underlayer. The mechanism of imaging was claimed to involve melting of the metal layer followed by metal coalescence, which loosened the ink adhesive layer.

To somewhat simplify the scope of the problem, we have chosen to study a relatively well-characterized model system suitable for dry offset lithographic imaging, in which the image is produced with a pulse from a single transverse mode (TEM₀₀) Nd:YAG laser operating at 1.064- μ m wavelength. We chose to concentrate on YAG rather than diode lasers, because the much higher power of the YAG (8 W) allows us to investigate a much wider range of imaging conditions, e.g., larger spot sizes, above threshold behavior, than the lower power diode lasers (<1 W). The direct imaging silicone plate system studied here differs from the materials mentioned before in two critical ways. First, a strong chemical interaction exists between the ink adhesive layer (silicone polymer) and the metallic underlayer (titanium and its oxides), which produces an extremely tough, durable, and strongly adherent coating suitable for extended commercial press runs ($\geq 100,000$ copies). Second, as we show next, the mechanism of removing the strongly adherent ink adhesive layer involves vaporization of the layer itself, rather than a physical or chemical process in the underlayer.

The essential elements of the model system are shown in Fig. 1. It is a monolithic three-layer film. The support is a polyester (PET) substrate, which is oleophilic. A thin film near-IR absorbing interlayer of nanometer thickness is deposited on the substrate. An oleophobic surface layer of micrometer thickness is applied over the interlayer. The film is exposed using single near-IR pulses with Gaussian spatial profiles, incident on the interlayer from the substrate side. Exposure causes a portion of the oleophobic surface layer to debond from the underlayers. After exposure, the film is treated by a simple physical postimaging

Original manuscript received August 1996.

* IS&T Member

† To whom correspondence should be addressed

© 1997, IS&T—The Society for Imaging Science and Technology

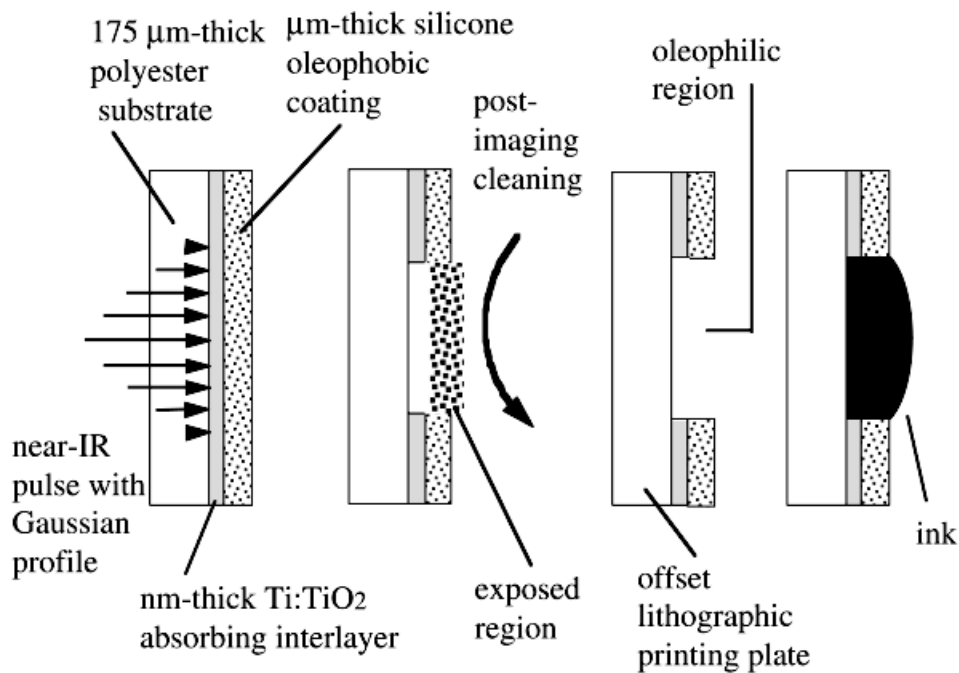


Figure 1. Schematic diagram of the film that is used for lithographic offset printing, imaged by a near-IR Gaussian profile pulse. About 50% of the pulse is absorbed at a thin interlayer. Debonding of the silicone coating from the polyester substrate creates an oleophilic well that attracts printer inks.

cleaning process, which removes the surface layer in the irradiated region, producing a “dot” where the PET substrate layer is exposed to the surface. Dots developed in this manner show an affinity for ink, due to the large differential oleophobicity and oleophilicity of the silicone and PET layers, respectively.⁴ A pattern of these dots produced by scanning the laser over the plate surface collectively forms the desired image. The resolution of an image produced on the film is primarily determined by the radius of the exposed dot. The dot radius itself is dependent on the radius and energy of the laser pulse. Under the conditions used here, dots were produced 5 to 30 μm in radius.

The exposed and cleaned film is suitable for some lithographic applications, but the model system differs a bit from actual production plates. In the PEARL™ system, usually the film is laminated to a metal plate suitable for mounting to a press,^{4,5} and the film is exposed by diode lasers incident from the coating face. Several alternative formulations, similar in spirit to this model system, have also been developed by Presstek, Inc.^{4,5} For example, the materials described here can be directly coated onto metal printing plates, and hydrophilic coating materials have been developed that are suitable for wet offset lithographic applications.⁴

The mechanisms of image formation are studied using two experimental techniques. In the first, the films are exposed to laser pulses at various intensities to investigate their threshold exposure properties.^{6,7} In the second, an ultrafast microscope apparatus^{7,8} is used to produce a “stop-action” stream of images of the exposure process during, and subsequent to, a 10-μs pulse. A theoretical model is presented that can be used to estimate the temperature in the film during the laser pulse, and to predict the radius of the exposed spot under different conditions of laser irradiation.

Experiments

Film. The substrate was 175-μm-thick (7 mil) PET. The near-IR absorbing interlayer was produced by sputtering titanium metal onto the substrate to a thickness estimated at 30 nm. The interlayer is believed to contain titanium

oxides as well as metallic Ti. The oleophobic surface layer consisted of a silicone polymer at a coverage of ~2 g/m². From this coverage, we estimate the thickness of the silicone layer to be in the 2 to 3-μm range. Details of the silicone coating material and coating process can be found in Ref. 1. After exposure, the films were gently cleaned using a cotton pad moistened with a bit of rubbing alcohol (isopropanol).

The fraction of incident near-IR light absorbed by the film was determined as follows. An absorption spectrophotometer with near-IR capability was used to measure the fraction transmitted T . The fraction reflected R was measured using weak unfocused 10-μs pulses from the YAG laser described next. A large area thermopile (Scientech Corp., model 360) with an accuracy of a few percent was used to measure the incident laser power and the power reflected from a film inserted in the beam at a small angle (~10 deg) to the normal. The fraction absorbed, η , was determined using the relation

$$\eta = 1 - T - R. \quad (1)$$

This measurement technique is not sensitive to reflected light, which is scattered at large angles. Prior studies⁹ comparing this method to the use of an integrating sphere, which captures all reflected light, showed that errors due to neglect of large angle scattering are negligible.

Exposure Source. A block diagram of the apparatus is shown in Fig. 2. The exposure source is a continuous-wave (cw) Nd:YAG laser (Quantronix Corp., Smithtown, NY, model 116), which produces 8 W in a TEM₀₀ beam. A 40-MHz acousto-optic modulator (IntraAction Corp., Bellville, IL, model AOM-40) is used to slice a 10-μs duration pulse from the laser output. The rise and fall times (10 to 90%) of the pulse are about 1.3 μs. The pulse energy is controlled using a variable attenuator consisting of a half-wave plate and two thin film polarizing beamsplitters (CVI Corp., Albuquerque, NM). The pulse energy is determined by setting the modulator repetition rate to a high repetition frequency of 5 KHz and measuring the average power with the thermopile. The film is

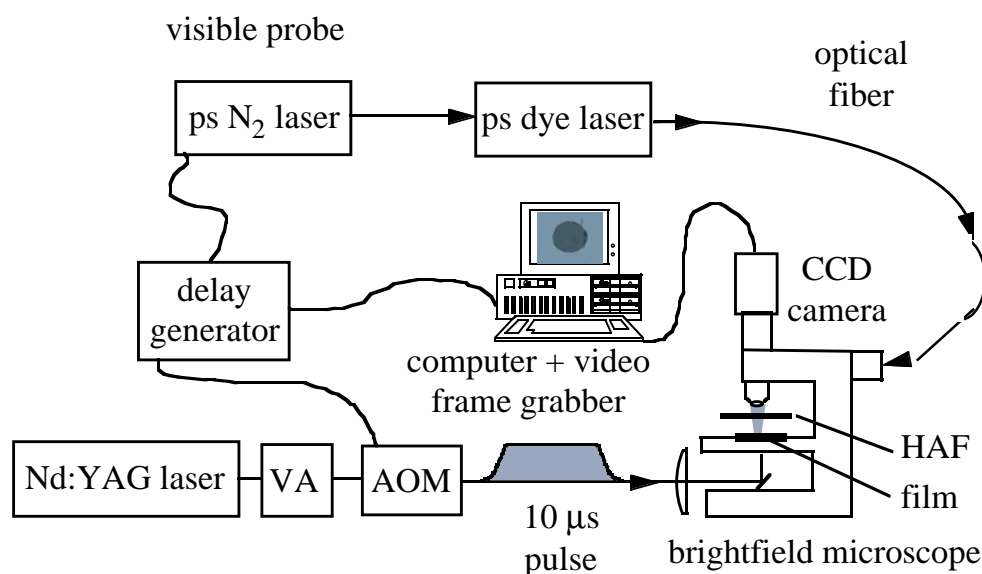


Figure 2. Block diagram of experimental apparatus used for time-resolved imaging of films irradiated by 10- μ s duration pulses. VA = variable optical attenuator; AOM = acousto-optic modulator; HAF = heat absorbing optical filter; and CCD = video camera with charge-coupled detector.

placed on the stage of an optical microscope with the silicone coating facing the objective. The film is irradiated from the substrate side by a focused near-IR pulse, which is directed to the stage by a mirror. A heat-absorbing optical filter (Hoya Corp., model HA-30) is placed between the film and the microscope optics. This filter absorbs the near-IR pulses while transmitting visible observation light.

The Gaussian beam diameter was measured using the knife-edge method.¹⁰ A translation stage with a differential micrometer with better than 1- μ m accuracy (Newport Corp., Irvine, CA, model DM-05) is used to scan a sharp razor blade in the focal plane across the laser beam. The transmitted laser pulses are monitored using a silicon photodiode and a digital oscilloscope, and the beam parameters are obtained by fitting the transmission data to an error function. Two Gaussian beam radii were used, either $r_0 = 18 (\pm 1)$ or $r_0 = 34 (\pm 1)$ μ m. The confocal parameter, a measure of the collimation length of the beam,¹⁰ is given by $b = 2\pi r_0^2/\lambda$. Thus b was either 1.7 or 6.8 mm, so small errors (on the order of a few 10 μ m) in determining the location of the focal plane were tolerable.

Ultrafast Microscope. The film is observed using a microscope (Olympus Corp., Melville, NY, model BX60M) in the bright field reflected light mode. A CCD camera (Sony Corp., model SSC-M254), a personal computer with a digital frame grabber (Data Translation, Marlboro, NH, model DT-2804A), and image acquisition and analysis software (Data Translation Global Lab Image™) were used.

For time-resolved microscopy, the tungsten lamp in the microscope was replaced by a pulsed dye laser, which provides a pulsed observation source. A high pressure nitrogen laser (Laser Photonics Corp., model LN203C), which produces a 100- μ J, 600-ps duration pulse at 337-nm wavelength, pumped a home-built dye laser using Coumarin 500 dye (Exciton Corp., Dayton, OH). Dye lasers pumped in this manner are said to produce a 300 to 500-ps pulse.¹¹ The dye laser pulse energy was 10 to 15 μ J, and its spectrum was a broadband (~ 30 nm) centered around 500-nm wavelength. The motivation for using a broadband laser with a short coherence length is to minimize coherent imaging artifacts such as laser speckle and interference fringes. The dye laser pulse was ported to the microscope by a 400- μ m-diam optical fiber. Although the fiber is expected to somewhat stretch the pulse dura-

tion, measurements using a Si photodiode (response time ~ 1 ns) showed the pulsed illumination source duration remains < 1 ns.

Time-resolved microscopy measurements were made as follows. The CCD camera and frame grabber run at 30 frames/s via synchronization to the 60-Hz line voltage. A pulse from the grabber, which occurs at the top of each frame, is used to trigger a home-built delay generator connected to the dye laser and the acousto-optic modulator. The relative delay between near-IR and dye laser pulses was measured with a fast digital oscilloscope (Tektronix Corp., Beaverton, OR, model 2440A) and a Si photodiode. In specifying delay times, we define $t = 0$ to be halfway up the rising edge of the 10- μ s near-IR pulse.

Notice this microscopy method obtains only a single stop-action stroboscopic image each time the laser is fired and the film is exposed. It is possible to reconstruct a series of images into a "motion picture" of the irradiated film, provided the exposure process is reproducible. The exposure process was quite reproducible, except for occasions when dust in the air floated through the laser beam, a small imperfection in the coating was exposed, etc. A certain amount of editorial discretion is inevitable in the reconstruction process. To make the process as objective as possible, and to verify that images displayed here are representative of the exposure process, images were obtained in sets of three at each delay time, and unusual or unrepresentative images were discarded.

Theory

In this section we discuss a model for exposure of a film with a sharp exposure threshold, using optical pulses with a Gaussian spatial profile. Then we discuss a thermal conduction model, which allows calculation of the temperature in the film.

Spot Size Model. Consider a film irradiated by a Gaussian spatial profile pulse with radius r_0 (the $1/e^2$ intensity radius). The fluence for a pulse with energy E_p delivered to a location on the film a distance r from the beam center at $r = 0$ is given by^{7,10}

$$J(r) = \frac{2E_p}{\pi r_0^2} \exp(-2r^2/r_0^2) = J(0) \exp(-2r^2/r_0^2). \quad (2)$$

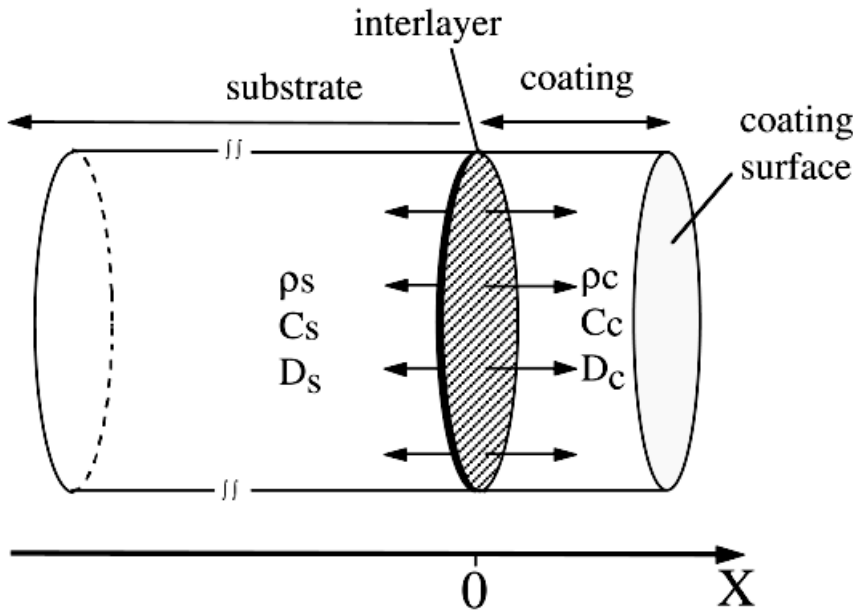


Figure 3. Schematic of simplified one-dimensional heat conduction model. The heat source is the thin absorbing interlayer at $x = 0$. The coating and substrate have thermal diffusivity, heat capacity, and density (D_c, C_c, ρ_c) and (D_s, C_s, ρ_s), respectively.

Equation 2 shows the fluence decreases rapidly with distance from the beam center. Now it is assumed the film has a sharp fluence exposure threshold J_{th} . When the fluence at the center of the beam $J(0)$ barely reaches threshold, $J(0) = J_{th}$, the film becomes exposed in a tiny region at the beam center. If the pulse energy is further increased, a larger spot is produced. The radius of the exposed spot r_s is given by the well-known relation^{6,7}

$$\frac{r_s}{r_0} = \begin{cases} 0 & J(0) < J_{th} \\ \sqrt{\frac{1}{2} \ln \left[\frac{J(0)}{J_{th}} \right]} & J(0) \geq J_{th} \end{cases} \quad (3)$$

Writing Efficiency. It is desired to minimize the number of expensive laser photons needed to expose the film. Suppose a spot with radius r_s is needed. This could be done using a larger laser beam radius ($r_0 > r_s$) and a lower fluence just above J_{th} , or a smaller laser beam radius ($r_0 < r_s$) and a larger fluence. It is possible to determine the minimum energy needed to produce a spot of radius r_s for a system which obeys Eqs. 2 and 3 by setting $(\partial E_p / \partial r_0)_{r_s} = 0$. The result is:

$$\begin{aligned} r_0 &= 1.414 r_s \\ E_p &= 2.718 J_{th} \pi r_s^2 \end{aligned} \quad (4)$$

Equation 4 defines the ‘‘point of maximum efficiency.’’ This condition occurs when the fluence at the center of the beam is 2.718 times the threshold fluence. The radius r_s of the exposed spot in that case is 0.707 times smaller than the laser beam radius r_0 .

Thermal Conduction Model. A model for heat conduction in the film is developed in this section. By introducing certain simplifications, we obtain a simple and useful analytical expression. However, the temperature calculation does not accurately describe what happens in the film

after the coating begins to debond. The model is shown schematically in Fig. 3. A thin interlayer of high thermal conductivity material is sandwiched between two thicker, lower conductivity materials. For common polymers, the thermal diffusivity D is of the order $D \sim 10^{-3} \text{ cm}^2/\text{s}$ (Table I). It will be useful in subsequent discussions to remember that on the 10- μs timescale of the near-IR pulse, the thermal diffusion length Λ_D in a polymer is about 1 μm , using the approximation¹² $\Lambda_D \approx (Dt)^{1/2}$.

One might use a finite element computational method to solve the diffusion equation for this system, as in Refs. 9 and 13, to provide the complete temperature distribution at all times and locations in the film. However, prior experience with such systems shows it is satisfactory to determine just the peak temperature and its location.^{9,13} That is because thermochemistry of polymers is extremely sensitive to temperature,¹⁴ and the most significant effects occur at the location of the temperature maximum. In the model described by Fig. 3, it is possible to obtain a compact and extremely useful analytical expression for the peak temperature under the following assumptions.

Only the Interlayer is Heated. The substrate and coating materials have no significant absorption in the near IR. By contrast, common interlayer materials absorb 30 to 50% of the incident near-IR radiation. The interlayer used here absorbs 50% of the incident light.

Interlayer is a Uniform Thin Heat Source. The surface of the interlayer facing the laser is heated more than the side facing away from the laser, due to attenuation of the pulse as it passes through the interlayer. But the interlayer is thin (about 100 times thinner than the coating) and it consists of materials such as Ti and TiO whose thermal diffusivities are more than ten times greater than the polymers (Table I). Thermal gradients created in the interlayer relax much faster than the time for heat transfer from interlayer to polymer layers.

One-Dimensional Conduction. On the timescale considered, heat can diffuse about 1 μm through polymers. That length scale is highly significant for diffusion from the interlayer to adjacent polymer layers, i.e., along the laser propagation direction (longitudinal conduction, see Fig. 3), but not very significant for diffusion perpendicular to the

TABLE I. Parameters used for Temperature Calculations

	density ρ	heat capacity C_p	thermal conductivity κ	diffusivity D
silicone ^{a)}	0.98 g/cm ³	1.53 Jg ⁻¹ deg ⁻¹	1.5×10^{-3} Js ⁻¹ cm ⁻¹ deg ⁻¹	0.98×10^{-3} cm ² s ⁻¹
PET ^{a)}	1.49 g/cm ³	1.13 Jg ⁻¹ deg ⁻¹	2.8×10^{-3} Js ⁻¹ cm ⁻¹ deg ⁻¹	1.86×10^{-3} cm ² s ⁻¹
Ti ^{b)}	4.5 g/cm ³	0.52 Jg ⁻¹ deg ⁻¹	2×10^{-1} Js ⁻¹ cm ⁻¹ deg ⁻¹	8.49×10^{-2} cm ² s ⁻¹
TiO ₂ ^{b)}	4.2 g/cm ³	0.59 Jg ⁻¹ deg ⁻¹	6.5×10^{-2} Js ⁻¹ cm ⁻¹ deg ⁻¹	2.5×10^{-2} cm ² s ⁻¹

^{a)} Data obtained from Ref. 21.

^{b)} Data obtained from Ref. 20.

laser propagation (transverse conduction) because the spot radius is typically $>10 \mu\text{m}$. Heat can diffuse farther through the metallic interlayer than through polymers, but the heat capacity of the thin interlayer is very small, which limits its ability to transport significant amounts of heat in the transverse direction.

Diffusion Length does not Exceed Twice the Coating Thickness. Our model concerns diffusion into an infinite thermal sink, but in the actual film the coating has a finite thickness. When heat from the interlayer reaches the coating surface (Fig. 3), the temperature at that surface builds up faster than predicted. This surface effect begins to affect the temperature at the interior of the coating and eventually at the interlayer. Deviations from our model appear when the diffusion length is twice the coating thickness. During the 10- μs period considered here, the diffusion length is $\sim 1.0 \mu\text{m}$ and twice the coating thickness is ~ 4 to $6 \mu\text{m}$. It is straightforward to correct our model for the finite coating thickness, but this additional complication is not needed here.

Optical Properties of the Interlayer Remain Constant. As the interlayer grows hotter, its optical properties may change, especially if it melts. In prior work,⁹ optical properties were studied of an aluminum interlayer in an ablation transfer film, irradiated by 150-ns pulses. The reflection and transmission of that interlayer did not change significantly during the pulse until ablation threshold was reached. Since the 10- μs pulses used here are considerably less intense than those used in the cited work, and Ti has a much higher melting point than Al, this assumption seems adequate, at least up to the onset of debonding.

Film Remains Intact. When the film is exposed above threshold, the coating layer begins to debond from the interlayer. Debonding radically affects thermal conduction between interlayer and coating, so after debonding our model becomes quite inaccurate. In comparison to results predicted by the model, the coating will be heated less and the interlayer temperature will climb much more rapidly once the interlayer stops losing heat to the coating.

Heat Capacity is Independent of Temperature. This is a problematic assumption, which simplifies our analysis greatly. Polymer heat capacities generally increase slightly with increasing temperature until thermochemical decomposition begins. When decomposition begins, the heat capacity increases greatly.¹⁵ Most available data on polymer thermochemistry is obtained at low heating rates, which does not provide a realistic view of what is happening at the enormous heating rate used here, $dT/dt > 10^7$ deg/s. Thermal decomposition at high heating rates can be vastly different than at low heating rates.^{15,16} A recent study¹⁶ using an ultrafast optical method showed the onset of thermal decomposition in PMMA was moved from $\sim 225^\circ\text{C}$ at low heating rate to $\sim 550^\circ\text{C}$ when dT/dt was $\sim 5 \times 10^9$ deg/s. We expect a temperature-independent heat capacity to slightly overestimate the polymer temperature prior to thermochemical decomposition, by ignoring the slight increase

in heat capacity with increasing temperature. When thermal decomposition begins, the actual polymer heat capacity will increase greatly, and the model will begin to radically overestimate the polymer temperature.

Summary. This model will provide reasonable results on the 10- μs time scale of the laser pulse, although it will overestimate the temperature a bit. Once the coating begins to decompose and debond from the interlayer, the calculation becomes unrealistic.

Analytical Expression for Temperature. Consider a laser beam with intensity I (W/cm²) that is turned on at time $t = 0$ and turned off at time t_p . A constant fraction η of the pulse is absorbed by the thin interlayer at $x = 0$. Heat is lost from the interlayer into a coating with density, heat capacity, and thermal diffusivity ρ_c , C_c , D_c , and a substrate with ρ_s , C_s , and D_s (Fig. 3). A one-dimensional diffusion equation¹² subject to the assumptions given before was written and solved with boundary conditions that require temperature T and gradient dT/dx to be continuous at the interlayer. It was then found the temperature in the coating increases during the near-IR pulse to a maximum value that occurs at the end of the pulse at time t_p . The location of the temperature maximum always occurs in the polymer adjacent to the interlayer at $x = 0$. The temperature at this location at any time t during the pulse is found to be

$$T(0,t) = \frac{2I\eta t}{\rho_c C_c \sqrt{(\pi D_c t)^{1/2}} + \rho_s C_s \sqrt{(\pi D_s t)^{1/2}}} \quad (5)$$

$(0 \leq t \leq t_p)$.

Figure 4 shows some sample calculations for the temperature during a 10- μs duration pulse using values for ρ , C , and D from Table I. This figure will be discussed in more detail later.

Results

Properties of the Interlayer. The interlayer from a strip of film was digested using nitric acid, and the solution was analyzed for Ti content by atomic emission spectroscopy. The result showed the minimum Ti coverage (some of the interlayer might not have been dissolved) to be 64 mg/m². Assuming theoretical maximum density, which gives an absolute lower limit to the thickness, that would correspond to a layer of pure Ti metal 14 nm thick or a layer of TiO₂ 25 nm thick. The film transmission was found to be $T = 0.30 (\pm 0.01)$ and the film reflection was $R = 0.19 (\pm 0.01)$. Using Eq. 1, the fraction absorbed was found to be $\eta = 0.49 (\pm 0.02)$.

Exposure Threshold. Figure 5 shows exposure threshold data at two values of the Gaussian beam radius, $r_0 = 18 \mu\text{m}$ and $r_0 = 34 \mu\text{m}$. The film was exposed to 10- μs pulses at different fluences, cleaned with rubbing alcohol, and examined in the microscope to determine the radius of the

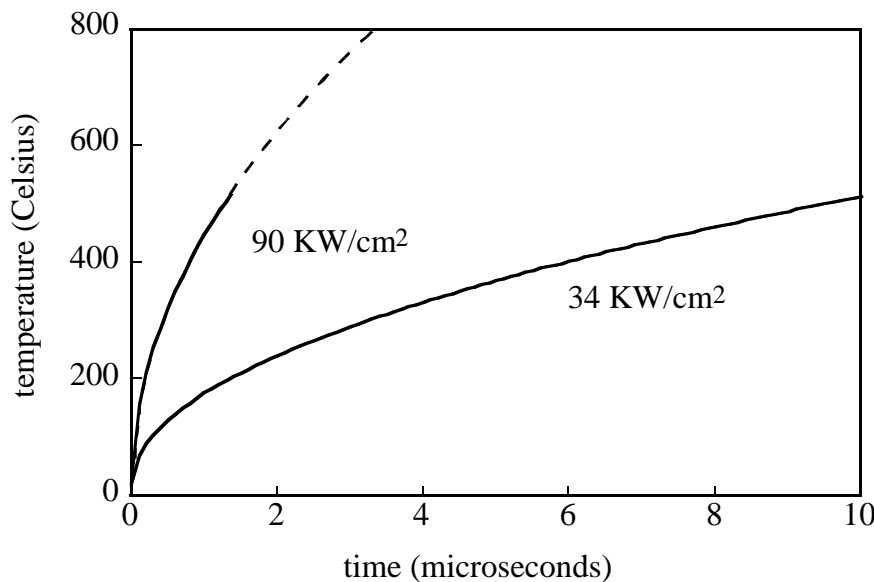


Figure 4. Computed temperature in the coating adjacent to the absorbing inter-layer during irradiation by a 10- μ s duration near-IR pulse. The 34 KW/cm² curve corresponds to irradiation at exposure threshold. The 90 KW/cm² curve describes above threshold irradiation at the center of the spot where the Gaussian beam is most intense. Above \sim 500°C, the calculations become unrealistic because the coating debonds from the underlayer. The unrealistic regime is denoted by a dashed extension of the calculated temperature curve.

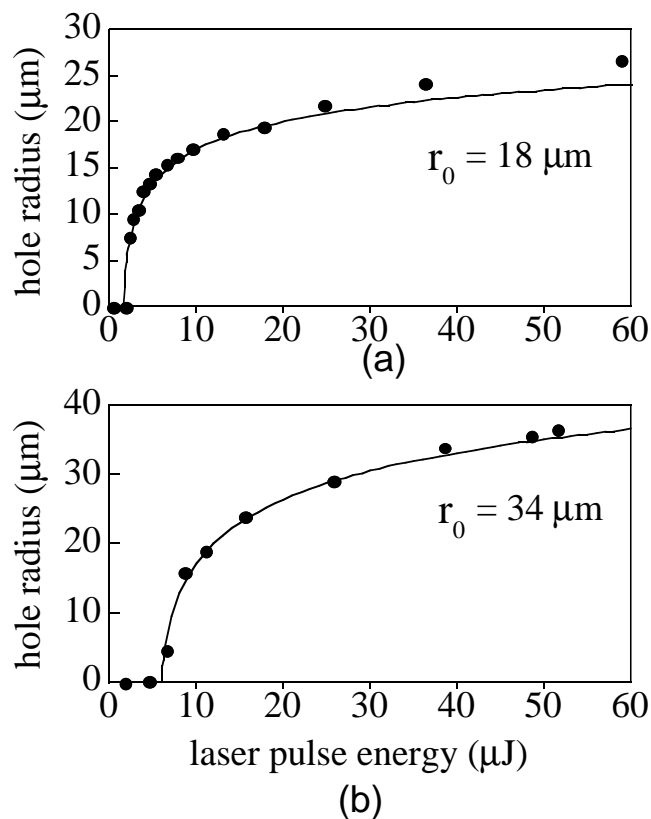


Figure 5. The solid circles denote the measured radius of exposed and cleaned spots in the film at the indicated values of laser pulse energy. The Gaussian beam radius is (a) 18 μ m or (b) 34 μ m. Both data sets are excellent fits to Eq. 3 (smooth curves), indicating a sharp exposure threshold of $J_{th} = 0.34$ J/cm², which is the same at both values of the beam radius.

exposed region. The smooth curves fit Eq. 3. The value of $J_{th} = 0.34 (\pm 0.02)$ J/cm² was obtained with both the larger and smaller beam radius. The fit to Eq. 3 is excellent. Error analysis shows the error in determining J_{th} is dominated by the experimental uncertainty in determining r_0 .

Exposed Spots. Figure 6 shows a series of spots exposed in the film using the $r_0 = 34$ - μ m diam laser beam before and after cleaning. These images were acquired using the larger 34 μ m beam radius because it is easier to see details in the larger spots. The data in Fig. 5 indicate that exposure behavior is essentially the same with the smaller spot size, so the data in Fig. 6 is representative of smaller spot sizes as well. Figure 6 shows that cleaning produces some scratches in the coating. The scratches do not penetrate the coating and do not affect the surface affinity for inks. Some experiments where the exposed films were rubbed gently or more vigorously showed the size of the exposed region was not critically dependent on how the cleaning was done.

The first image in Fig. 6 shows a film irradiated at a low fluence, which barely causes a detectable effect. In a small region near the beam center, the silicone coating develops tiny wrinkles. When this wrinkled area is cleaned, the silicone coating is not removed. By our criteria this fluence is deemed below exposure threshold. In the second image, a slightly higher fluence produces a larger wrinkled region with a small plateau in the middle. After cleaning, the plateau region is removed leaving a small exposed spot. Much of the wrinkled region remains after cleaning. By our criteria, this fluence is deemed slightly above exposure threshold. The third image is obtained after irradiation near the point of maximum efficiency. After cleaning, a nicely exposed spot is produced. The fourth image was produced with about twice the fluence as the third. At this higher fluence, much of the silicone coating is removed by the laser pulse itself, so little cleaning is required to remove what remains.

Wherever the coating was removable by cleaning, microscopic evidence indicated the titanium layer had been removed. An annulus of titanium metal seen at the perimeter of the exposed spots suggests the interlayer has melted and either receded¹⁷ from the exposed region, or coalesced into tiny (invisible by optical spectroscopy) metal beads.⁹

Time-Resolved Microscopy. A series of stop action images, taken during a 10- μ s pulse, is shown in Fig. 7. The beam radius $r_0 = 34$ μ m was used, and the pulse energy of 15 μ J is close to the point of maximum efficiency.

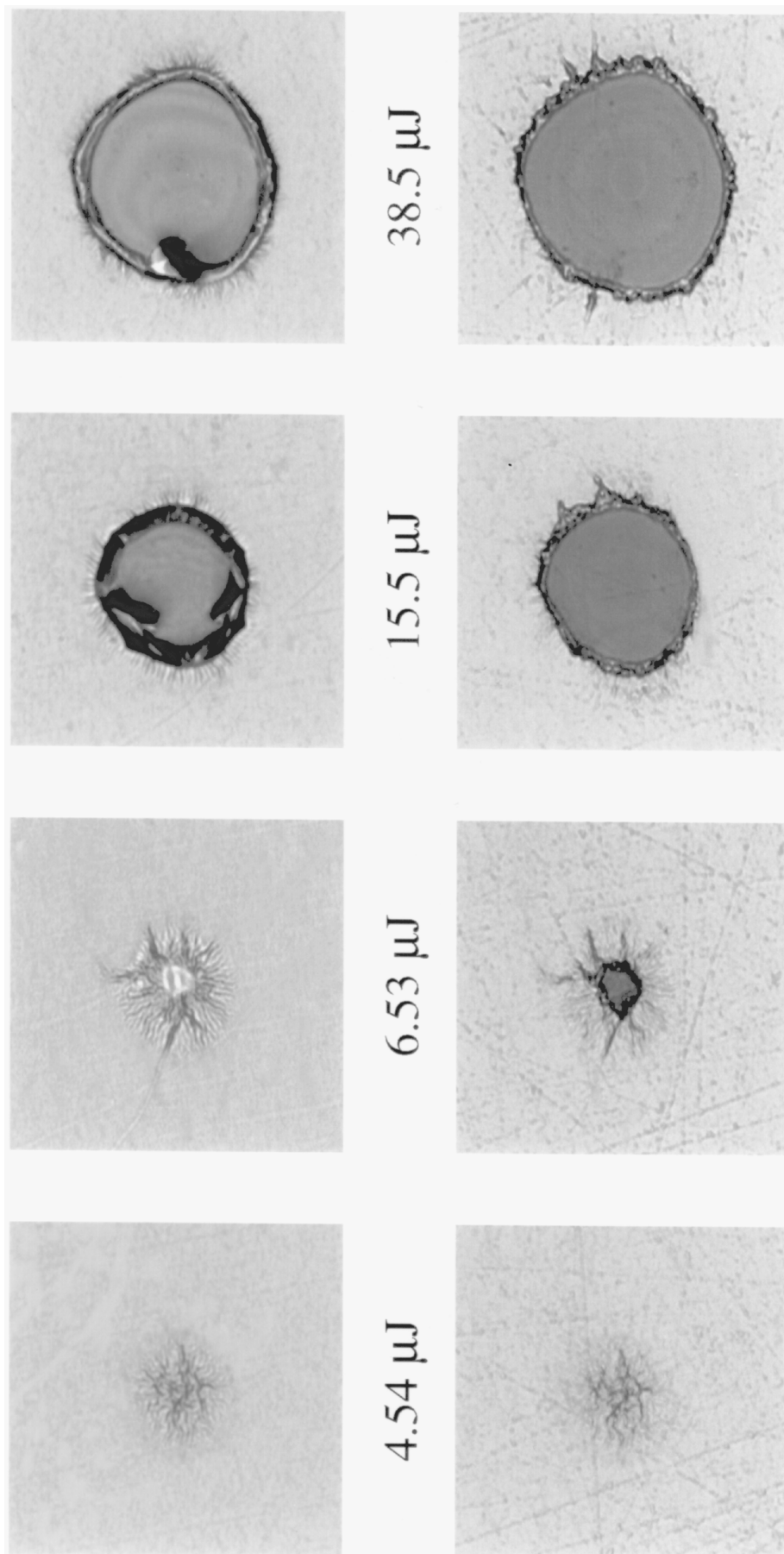


Figure 6. Examples of spots exposed in a film by a 10- μs duration pulse with a 34- μm diam Gaussian beam radius at the indicated pulse energies. The bottom row shows the same spots in the top row, following cleaning with rubbing alcohol.

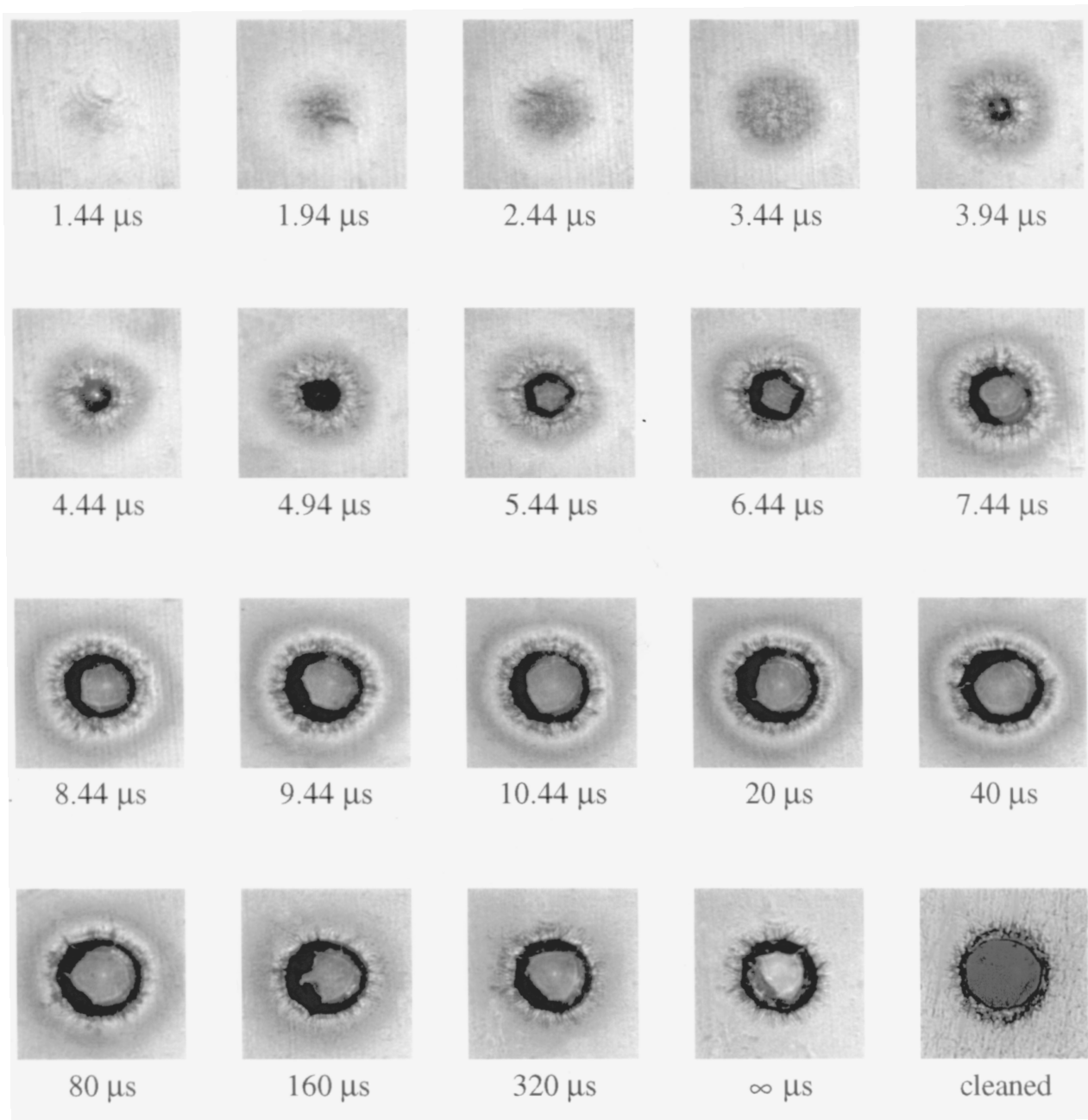


Figure 7. Stop action image sequence of a film being exposed by a 10- μ s duration near-IR pulse with a 34- μ m Gaussian beam radius under conditions close to the point of maximum efficiency.

At about 1.5 μ s, the first effects of the pulse are seen. A small wrinkled region is observed. For the next 2.5 μ s, the diameter of this wrinkled region increases and the center of the wrinkled region begins to puff up and lift off the film. At \sim 4 μ s, the center of the coating tears or bursts, leaving a hole in the middle. During the remainder of the 10- μ s pulse, the exposed region and the hole continue to grow and the coating continues to puff up. When the pulse ends at 10 μ s, the puffed up coating begins to settle back onto the substrate. After a long time (actually a few seconds, denoted as $t = \infty$ in the figure), the coating has finished settling and the exposed region appears quite irregular. Once the coating is cleaned, a nice reproducible exposed spot with a very sharply defined perimeter is seen.

Temperature Calculations. Temperature calculations were performed using Eq. 5 to describe irradiation at the point of maximum efficiency. At this point, the fluence at the edge of the exposed spot is exactly J_{th} , and the fluence at the center is $2.718J_{th}$. The intensities corresponding to these fluences are determined by dividing the fluence by the pulse duration t_p . For a 10- μ s duration pulse at threshold fluence $J_{th} = 0.34 \text{ J/cm}^2$, the intensity at the perimeter is $I = 34 \text{ KW/cm}^2$. The intensity at the center is $I = 90 \text{ KW/cm}^2$. Using the experimental value for the fraction of absorbed light $\eta = 0.5$, the temperature profiles shown in Fig. 4 were computed. Recall that these calculations give the temperature of the silicone coating adjacent to the absorbing interlayer. Figure 4 shows at the perimeter the

temperature rises to a peak of $\sim 500^\circ\text{C}$. At the end of the pulse, the temperature will begin to decline on the timescale of a few $10\ \mu\text{s}$ (not shown). At the center of the irradiated region, the temperature climbs more rapidly and reaches $\sim 500^\circ\text{C}$ at about $1.5\ \mu\text{s}$. The calculation then shows the coating temperature at the spot center continuing to increase rapidly. As discussed in the theoretical section, the calculation beyond this point is physically unrealistic due to the onset of thermochemical decomposition and debonding. The unrealistic region is denoted by the dashed extension of the curve in Fig. 5.

Discussion

The exposure of these multilayer films by Gaussian laser pulses is quite complicated. Our experiments show that the mechanism of removal of the ink adhesive layer involves thermochemical decomposition and the production of gas-phase decomposition products from that layer. Our experiments also provide insight into the physical processes that occur during exposure. It is not within the scope of this paper to describe in detail the chemical processes, although it is worth mentioning that fast coherent Raman¹⁸ and infrared¹⁹ techniques have recently been developed, which now allow real-time investigations of fast chemical reactions in thin polymer films during irradiation by intense near-IR pulses.

According to the calculations in Fig. 4, when the silicone coating is irradiated at threshold it reaches a maximum temperature of $\sim 500^\circ\text{C}$. It should be kept in mind that this is likely to be a bit of an overestimation of the actual debonding temperature, because we assumed a constant room temperature heat capacity and neglected the sudden increase in heat capacity when the polymer begins to decompose. One must also be concerned that the thermal diffusivity of the actual silicone coating might differ somewhat from the literature value in Table I. Fortunately the computed temperature is not highly sensitive to D_c , since it depends on $(D_c)^{-1/2}$.

It is hard to tell from the gray scale images in Figs. 6 and 7, but visual observation (in color) of films under the microscope shows that whenever the coating is removed, the interlayer is also absent. Despite the fact that the melting point of the interlayer materials greatly exceeds the calculated 500°C temperature, this can be explained as follows. Once debonding occurs, the interlayer stops losing heat to the adjacent polymer layers and it begins to be heated adiabatically. When a thin, strongly absorbing layer not in thermal contact with a larger mass is irradiated by a laser, its temperature increases very rapidly. To make our point, let us use the admittedly crude assumption that the interlayer consists of a 20-nm layer of pure Ti. Melting Ti at room temperature requires²⁰ about $5\ \text{kJ}/\text{cm}^3$. With adiabatic heating, the laser fluence needed to melt such a layer (which absorbs $\sim 50\%$ of the incident light) is about $0.02\ \text{J}/\text{cm}^2$. At the perimeter of the spot, the fluence is $0.34\ \text{J}/\text{cm}^2$ and at the center the fluence is $0.9\ \text{J}/\text{cm}^2$. Thus once debonding occurs, only a small fraction of the total energy is needed to melt the interlayer. When the interlayer has melted, surface tension will cause it to recede toward the spot perimeter,¹⁷ or to form tiny metal beads.⁹

Perhaps the most interesting observation is how accurately the exposure behavior of the film is described by the simple model of Eq. 3. The assumption underlying Eq. 3 is the existence of a very sharp exposure threshold. On initiation of this study, we did not see any *a priori*

reason why the threshold had to be so sharp. It was conceivable that the adhesion between the coating and the interlayer might take on a continuum of values depending on the pulse intensity. In that case the diameter of the exposed region would depend on the cleaning process. Gentle cleaning would produce a smaller exposed spot than harsh cleaning. However, that is not observed to happen. The size of the cleaned spot is highly dependent on the laser fluence and virtually independent of the cleaning process. In the exposed film, the adhesion is seemingly bimodal: either it is quite strong, or it is quite weak.

The prior discussion suggests a possible mechanism for the sharp threshold worth further investigation. Once the coating starts debonding even a little bit, the interlayer will abruptly melt, which suddenly destroys any remaining adhesion between coating and substrate. This positive feedback mechanism, or something similar, would tend to amplify the effects of a slight weakening in thermal contact between coating and interlayer. The all-or-nothing debonding behavior is highly desirable.

Another interesting observation is that the fluence threshold is independent of laser beam radius (at least in the $r_0 = 18$ to $34\ \mu\text{m}$ range). Equation 3 does not say anything about the spot size dependence of J_{th} , if indeed there is one. There is but a single necessary and sufficient condition for a lack of dependence on spot size: the exposure process at the perimeter of the spot, which ultimately determines the spot size, must not be affected by anything happening elsewhere on the film. For example, thermal conduction along the radial direction (see Fig. 3) could not be important in determining J_{th} because the cooling rate at the perimeter would depend on the spot radius.¹² One intriguing example of a mechanism that might lead to a spot-size dependent threshold is suggested by Fig. 7. As the coating puffs up and lifts off the center of the spot, it might tug on the coating at the perimeter. That could reduce the fluence needed to debond the perimeter coating. Small spots where the perimeter was close to the center would have a lower threshold than large spots. That this is not observed to happen might be related to the hole at the center of the coating (see $t > 4\ \mu\text{s}$ in Fig. 7). Once the hole forms, the hot gas tends to escape, which limits its ability to affect the exposure process occurring at the perimeter.

We end this section with one more noteworthy observation. Looking at the exposure of the spot center shows how a film reacts to intense laser pulses above threshold. With more intense pulses, the fluence at the spot center reaches the threshold fluence J_{th} well before the $10\text{-}\mu\text{s}$ pulse ends. Observing the spot center thus might provide insight into the effects of using shorter duration exposure pulses. There are two ways a film might react to shorter pulses. The film might evidence reciprocity, in which case the threshold fluence will not depend on pulse duration. Alternatively, the threshold fluence might depend on pulse duration. For example, the coating might always debond at any pulse duration when the temperature at the interlayer-coating interface reached a particular temperature, in this case $\sim 500^\circ\text{C}$. Equation 5 shows it takes less energy to reach this temperature with a shorter pulse, so if this supposition proved to be the case, the threshold fluence would decrease with decreasing pulse duration.

Using the time-resolved images in Fig. 7, we can hazard an educated guess as to how the film will react to shorter pulses. If reciprocity held for this film, the central coating would begin to debond as soon as it has received $J_{\text{th}} = 0.34\ \text{J}/\text{cm}^2$. In Fig. 7, the fluence at the center is about 2.718

times threshold, so debonding would occur in the reciprocity case at about 3.7 μs . On the other hand, Fig. 4 shows the center reaches the desired temperature of $\sim 500^\circ\text{C}$ at about 1.5 μs . Now we look at Fig. 7 and attempt to judge when debonding has first begun at the center. Figure 7 suggests debonding at the center is first observed well before the 3.44- μs frame, perhaps as early as 1.44 μs , and certainly by 1.94 μs . At 1.94 μs , for example, the fluence received at the center was $J \approx 0.17 \text{ J/cm}^2$, a factor of two less than the threshold fluence. Therefore this argument indicates the threshold fluence decreases considerably, when more intense, shorter duration pulses are used. In prior work on laser ablation imaging,¹³ an order of magnitude decrease in exposure fluence was seen going from 10^{-7} to 10^{-10} s pulses. From the data presented here, we may infer that shortening the pulse duration from 10 μs to 1.5 μs decreased the threshold by roughly a factor of 2. Possibly further decreasing the pulse duration will further decrease the threshold. Decreasing the exposure threshold is highly desirable in the bulk of commercial applications. A more detailed study of the pulsewidth dependence of the exposure threshold reduction in the 10^{-5} to 10^{-13} s range is currently in progress. \blacktriangle

Acknowledgment. The work at the University of Illinois was supported by a grant from Presstek, Inc. Acknowledgment is made for partial support from the National Science Foundation, grant DMR 94-04806, and the US Army Research Office, contract DAAH04-96-1-0038 (to D. D. D.).

References

1. N. Nechiporenko and N. Markava, *Proceedings of 15th International IARIGAI Conference*, Lillehammer, Norway, 1979, p. 139.
2. A. C. Eames, Canadian patent 1050805, (Mar. 20, 1979).
3. L. Leenders and H. Peeters, Research Disclosure 1920, April 1980, p. 131.
4. T. E. Lewis, M. T. Nowak, K. T. Robichaud, and K. R. Cassidy, US patent 5,339,737 (Aug. 23, 1994).
5. T. E. Lewis, M. T. Nowak, and K. T. Robichaud, US patent 5,353,705 (Oct. 11, 1994).
6. D. Maydan, *The Bell System Technical Journal* **50**, 1761 (1971).
7. I.-Y. S. Lee, W. A. Tolbert, D. D. Dlott, M. M. Doxtader, D. M. Foley, D. R. Arnold, and E. W. Ellis, *J. Imag. Sci. Tech.* **36**, 180 (1992).
8. H. Kim, J. C. Postlewaite, T. Zyung, and D. D. Dlott, *J. Appl. Phys.* **64**, 2955 (1988).
9. W. A. Tolbert, I.-Y. S. Lee, D. D. Dlott, M. M. Doxtader, and E. W. Ellis, *J. Imag. Sci. Tech.* **37**, 411 (1993).
10. A. E. Siegman, *Lasers*, University Science Books, Mill Valley, CA, 1986.
11. This specification was provided by Laser Photonics, Inc., Orlando, FL.
12. G. Barton, *Elements of Green's Functions and Propagation. Potentials, Diffusion and Waves*, Clarendon Press, Oxford, 1989.
13. W. A. Tolbert, I.-Y. S. Lee, X. Wen, M. M. Doxtader, E. W. Ellis and D. D. Dlott, *J. Imag. Sci. Tech.* **37**, 485 (1993).
14. J. H. Flynn, in *Thermal Analysis in Polymer Characterization*, E. A. Turi, Ed., Heyden & Son, Inc., Philadelphia, 1981, pp. 43–59.
15. O. F. Shlensky, A. A. Matyukhin and E. F. Vaynshteyn, *J. Thermal. Anal.* **31**, 107 (1986).
16. I.-Y. S. Lee, X. Wen, W. A. Tolbert, D. D. Dlott, M. M. Doxtader, and D. R. Arnold, *J. Appl. Phys.* **72**, 2440 (1992).
17. F. Spaepen and D. Turnbull, in *Laser Annealing of Semiconductors*, J. W. Mayer, Ed., Academic Press, New York, 1982, Chap. 2.
18. D. E. Hare and D. D. Dlott, *Appl. Phys. Lett.* **64**, 715 (1994).
19. T. Lippert and P. O. Stoutland, *Proceedings of IS&T 49th Annual Conference*, Soc. Imag. Sci. Tech., Springfield, VA, 1996, p. 484.
20. *CRC Handbook of Chemistry and Physics*, 61st ed., CRC Press, Boca Raton, FL, 1981.
21. D. W. Van Krevelen, *Properties of Polymers*, Elsevier, Amsterdam, 1990.